Integrity Monitoring of Right-Angle Structures Using Metamaterial Assisted Guided Wave Mode Discrimination

XIAOLEI XU, YANPING ZHU and FUCAI LI*

Xiaolei Xu, The State Key Laboratory of Mechanical System and Vibration, Shanghai Jiao Tong University, 800 Dongchuan Rd., Shanghai 200042, China
Yanping Zhu, School of Information Science and Technology, Beijing University of Technology, 100 Pingleyuan, Chaoyang District, Beijing 100124, China
Fucai Li*, The State Key Laboratory of Mechanical System and Vibration, Shanghai Jiao Tong University, 800 Dongchuan Rd., Shanghai 200042, China

ABSTRACT

This study proposes a novel method for structural integrity monitoring of right-angle structures, such as welded joints and T-profile panels, using ultrasonic guided waves. Firstly, building on the observed phenomenon of transmission and reflection selectivity of guided wave modes at geometric discontinuities, a framework for discontinuity detection is developed. Secondly, to address the issue of the damage-sensitive mode wave packets being immersed by other wave mode energy, a metamaterial-based mode selection design is proposed. The designed metasurface with a distinct bandgap selectively filters and amplifies certain guided wave mode (S0), making it feasible to recognize the signal caused by small-scale defects within a single measuring point. Thirdly, a testbench based on a T-shape aluminum profile is constructed, with the experimental results confirming the effectiveness of this approach in improving damage detection accuracy. By integrating the two predesigned damage index and introducing the Huber regression estimator, structural integrity can be evaluated precisely. The proposed framework contributes to advancing SHM techniques, particularly for structures with challenging geometries, by combining ultrasonic metamaterials with guided wave mode discrimination.

INTRODUTION

Structural integrity inspection of right-angle structures, such as welded joints, pipe elbows, and T-profile panels, is of paramount importance across various industrial sectors, including aerospace, civil infrastructure, and petrochemical industries [1]. Accurate and reliable detection of defects in these structural components is essential to ensure operational safety, prolong service life, and prevent catastrophic failures.

Ultrasonic guided wave testing (UGWT) is widely adopted due to its capability for long-range, rapid, and sensitive defect detection [2]. Guided waves propagate along structural boundaries and can interact sensitively with defects, making them advantageous for inspecting large or complex geometries efficiently. However, UGWT faces significant challenges when applied to right-angle structures. Abrupt geometrical discontinuities, like those found in welded joints or pipe elbows, lead to complex mode transitions and reflections, causing significant interference and reduced defect detection capability. In particular, common-scale defects such as welding discontinuities often result in signals being dominated by primary wave modes, overshadowing critical defect indicators and thus limiting the quantitative evaluation of structural integrity.

Previous studies [3], [4] have observed the phenomenon of mode selectivity at geometric discontinuities, highlighting that guided wave modes exhibit distinct

transmission and reflection behaviors when encountering right-angle interfaces. Specifically, symmetric and antisymmetric wave modes undergo selective conversion and reflection at abrupt structural changes. This mode transition behavior has shown promise for qualitative assessment of structural discontinuities, but quantitative evaluation has remained challenging due to the dominance of primary modes obscuring the defect-sensitive signals.

Metamaterials are widely used in SHM fields in recent years for screening, enhancement, and isolation [5~7]. The mode-selective phenomenon of elastic metamaterials (EMMs) are revealed [8], which proves to be a potential tool for inspection under mode-discriminative circumstances.

In this study, we address these limitations by proposing a novel structural health monitoring (SHM) framework that integrates ultrasonic guided wave mode discrimination with acoustic metamaterials. First, we systematically analyze the mode transition phenomena through a rigorous theoretical framework based on Navier equations and boundary condition analysis. Second, we perform numerical simulations using finite element methods to verify the selective mode filtering and enhancement mechanisms. Third, we design and apply metamaterials with distinct bandgap characteristics to selectively filter out the coupling antisymmetric mode (A0) and amplify the defect-sensitive symmetric mode (S0), significantly enhancing the signal-to-noise ratios. Finally, experimental validation involving artificial defects in welded specimens confirms the effectiveness and practicality of our approach.

Results from both simulations and experiments clearly demonstrate increased sensitivity and improved accuracy in detecting and quantifying structural integrity, representing substantial advancement over traditional guided wave methods. By integrating advanced acoustic metamaterial designs with guided wave mode discrimination strategies, this research provides a robust and precise solution for the structural health monitoring of geometrically challenging right-angle components, offering significant contributions to nondestructive testing methodologies and practical engineering applications.

METHODOLOGY

A. Mode transition in right-angle structure

To investigate the propagation behavior of ultrasonic guided waves in right-angle structures, the following geometric model is established: in the inverted T-shaped plate, the transverse plate is aligned parallel to the X-axis, while the vertical plate is aligned parallel to the Y-axis, with the right-angle junction defined as the coordinate origin. The excitation point is positioned at one end of the transverse plate, as illustrated in Figure 1(a).

Taking the transmission behavior of the S0 mode as an example, in the transverse plate (aligned along the X-axis), the displacement of the S0 mode is primarily characterized by in-plane vibration. The corresponding displacement field and stress can be expressed as follows

$$u_x(x,t) = Ue^{i(kx-\omega t)} \tag{1}$$

and the corresponding normal stress is

$$\sigma_{xx} = E\frac{\partial u_x}{\partial x} = ikEUe^{i(kx-\omega t)} \tag{2}$$

in which, E is the Young's module, k is wave number and ω is the angular frequency.

In the right-angle joint (at the origin), when the stress σ_{xx} of the transverse plate acts on the vertical plate (along the Y-axis). Since the two plates are orthogonal, σ_{xx} in the vertical plate is converted to the bending moment around the Y-axis M_z. The bending moment is obtained by the stress integral along the thickness of the plate

$$M_z(0,t) = \int_{-\frac{h}{2}}^{\frac{h}{2}} \sigma_{xx}\, x\mathrm{d}x = ikEU\frac{h^2}{12}e^{-i\omega t} \tag{3}$$

in which, h is the plate thickness.

The bending vibration of the vertical plate is driven by the bending moment, which satisfies the Mindlin plate equation

$$D\frac{\partial^4 u_z}{\partial y^4} + \rho h\frac{\partial^2 u_z}{\partial t^2} = -M_z\delta(y) \tag{4}$$

in which, $D = Eh^3/12(1-\gamma^2)$ is bending stiffness, ρ is the density and $\delta(y)$ is the Dirac function, representing that the bending moment is set on the origin.

The solution of the equation is the bending wave (A0 mode) in the vertical plate, and its displacement form is

$$u_x(y,t) \propto e^{i(k_y y-\omega t)} \tag{5}$$

in which, the wavenumber k_y satisfy the dispersion relationship of

$$Dk_y^4 = \rho h\omega^2 \tag{6}$$

This solution corresponds to the out-of-plane vibration of the A0 mode, indicating that the in-plane stress of the S0 mode wave excites the vertical plate through the bending moment. A similar solution applies to the section of the propagation path located at the rear end of the vertical plate in the lateral direction.

For further investigation, a set of simulations using finite element methods (via COMSOL Multiphysics) is conducted. The T-shaped plate is constructed with both horizonal and vertical plate 4 mm in thickness. For simulating the infinite plate field, low reflection boundaries are set at every end of both plates. The material is selected as pure aluminum. The excitation point is set to x = 230.8 mm and the signal are set as 5-cycle sine wave modulated by Hanning window in f = 250 kHz, in which only A0 and S0 mode could exhibit theoretically. Meanwhile, the excitation points are set symmetrically at both sides of the plate to generate pure S0 mode wave.

Three observation routines I, II and III are defined for mode judgement, as labeled in each sub-figure. Discrete observation points are taken 0.5mm apart for each path and measured to generate wavenumber-frequency plots under 2D-fast Fourier transform (2D-FFT). For routine I, the direct wave pattern corresponds the pure S0 mode around the excitation frequency, as shown in Figure 1(b). For the routine II behind the vertical plate, A0 mode wave dominate in energy with relatively low-amplitude S0 mode wave detected, as shown in Figure 1(c). For routine III in vertical plate, the result shows similar mode transition and amplitude proportion as in routine II, which is shown in Figure 1(d). This transformation and decentralization of S0 mode wave also explains its failure in domination in routine II. The observed phenomenon shows strong accordance to the deduction of theoretical model, supporting that strong mode transition from S0 to A0 occurs at right-angle structure.

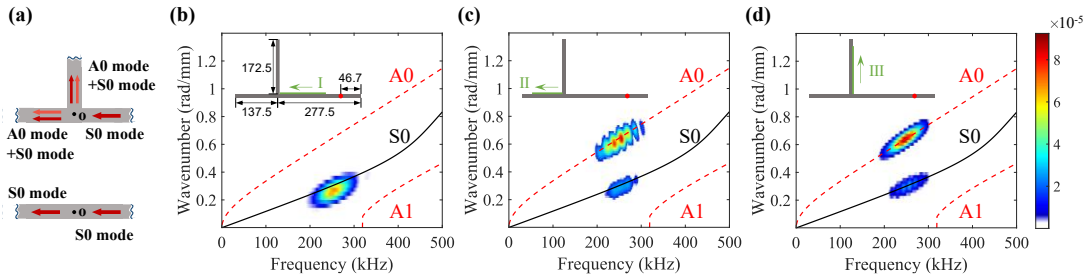

Figure 1 geometric model of T-shape right angle structure with schematic mode pattern labeled in (a), 2D-FFT analysis result for observation routine I, II and III in (b), (c) and (d)

Based on this specific ultrasonic guided wave propagation process in right-angle structures, a set of structural integrity monitoring frameworks could be established. Since the phenomenon of mode transformation could be weakened when there are discontinuous defects in the right-angle structure, the defect information can be reflected by monitoring the energy of certain wave mode in the vertical plate or the transverse path behind the plate. However, in a practical PZT-activated system, both symmetric and antisymmetric mode Lamb waves are inevitably excited, while the energy of either is sensitive to defect characterization. Meanwhile, traditional modality identification methods are usually based on simultaneous measurement of vast measurement points, which requires high hardware requirements (usually a laser doppler vibrometer). Therefore, it is urgent to develop a mode energy extraction method based on unilateral point to facilitate the inspection process.

B. Meta-surface design

To address the challenge of dominant mode interference and enhance defect-

sensitive signal detection, an acoustic metasurface is designed specifically targeting the suppression of the coupling antisymmetric (A0) mode energy. The metasurface is made up of a periodic, locally resonant unit with the combination of Ti-6Al-4V substrate with brass resonator. Such metasurface would perform both complete bandgap and bandgap for certain mode of waves, enabling the target mode to be detected though the structure.

Parametric analyses and topology optimization are performed to determine the optimal geometrical parameters, including lattice constants as 6 mm, resonator diameter d = 5 mm, and titanium alloy pillar height h_1 = 3 mm and copper height h_2 = 2 mm, ensuring precise tuning of the bandgap frequency range. Figure 2(a) illustrates the resulting bandgap curve along the Γ→X direction, clearly showing distinct bandgap for A0 mode which is later used as mode filter.

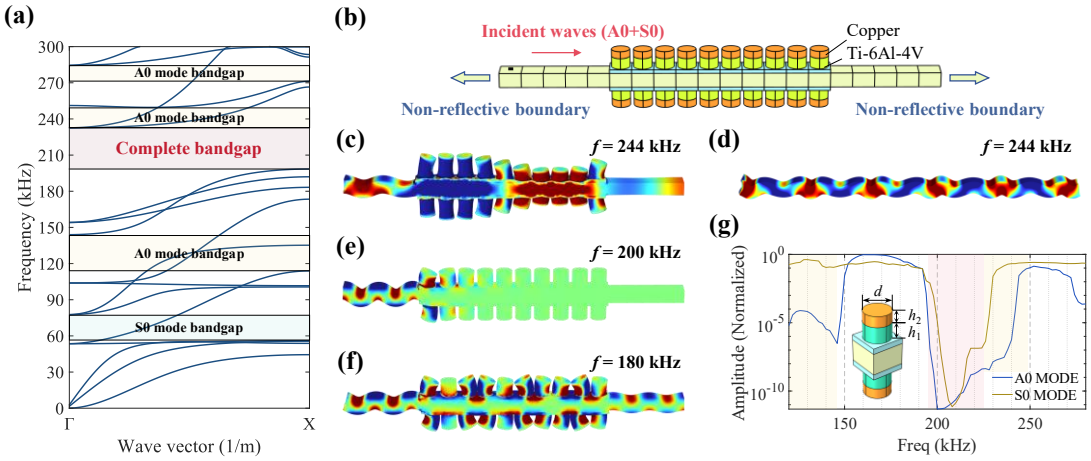

Figure 2 meta-surface overall design, including (a) bandgap curve in Γ→X direction, (b) FE model of a 10-unit-chain structure, (c) the equivalent stress response of the structure under 244 kHz and the response under same frequency without metamaterial in (d), (e) the equivalent stress response of the structure under 200 kHz and (f) the stress response of the structure under 180 kHz.

FE simulations were conducted on a 10-unit-chain metasurface structure, shown as Figure 2(b). Stress responses under different excitation frequencies were analyzed to validate the targeted selective filtering capability. An excitation frequency of 244 kHz (within the A-mode bandgap), the metasurface significantly reduces the equivalent stress, whereas the structure without the metasurface shows substantial stress propagation, as shown in Figure 2(c) and (d). Furthermore, Figure 2(e) illustrates the complete suppression at 200 kHz (within a complete bandgap), and Figure 2(f) indicates unhindered wave transmission at 180 kHz which is in the passband for both modes.

Figure 2(g) reveals the ratio of the measurement point amplitude and the excitation point amplitude on the posterior side of the metamaterial in the 120 kHz

to 280 kHz interval to reflect the modal passing rate at different frequencies. It can be found that the S0 and A0 modes exhibit extremely low passing rates in the complete bandgap, while the amplitude of the S0 mode is generally larger by at least 5 orders of magnitude in the A0 bandgap interval. This selective filtration has been validated experimentally, demonstrating improved defect detection capabilities in practical structural health monitoring scenarios.

IMPLEMENT & VALIDATION

A. Experimental Setup

In this part, an experiment is conducted to verify the applicability of the proposed framework. The test bench is composed of Tektronix TBS-2000B oscilloscope, AFG series function generator and ATA-4012 power amplifier. The test specimen is made of an integrally formed T-shaped 6061-aluminum profile. The horizontal plate has a length of 120 mm, the vertical plate has a length of 90 mm, and both plates have a thickness of 4 mm. Ultrasonic guided waves are excited at one end of the transverse plate and received by a PZT patch placed at the opposite end of the transverse plate, with the waves propagating through the right-angle structure and the metamaterial array designed in Chapter 2, as shown in **Figure 3(a)**.The meta-surface is manufactured by metal 3d-printing technology. The defect is designed as angle discontinuity with the scale range of 5~25 mm and realized by angle grinder, forming 13 different damage cases.

In this case, the excitation waveform is set as 8-period sine wave modulated by Hanning window under the frequency of 244 kHz (within A0 mode band gap). The amplitude is set as 5V and amplified by 10 times. Defects of varying scales are introduced and tested, of which the captured signal shown in **Figure 2(b)**. A similar waveform trend is observed across different cases. However, the captured amplitude varies, showing an overall increase with the expansion of the discontinuity length l_c. This observation verifies the feasibility of the proposed framework, which aims to manipulate the coherence between the intensity of mode conversion and the growth of structural discontinuity. To further form an index which indicates the defect severity, the root mean square of temporal signal is measured,

$$DI_{\mathrm{rms}} = \sqrt{\frac{1}{T}\sum_{0}^{T}(x^2(t) - y^2(t))\mathrm{d}t} \tag{7}$$

in which, T is the sampling duration. Meanwhile, the damage index based on the signal variance is defined,

$$DI_{\mathrm{var}} = \frac{1}{T}\sum_{0}^{T}(x(t) - \bar{x})^2 \tag{8}$$

in which, $\bar{x}$ is the mean value of the signal in the time period T.

The guided wave signals are captured under all damage scales, part of which shown in **Figure 3(b).** In intuitive observation, the amplitude magnifies with the increment of l_c, with a little phase shift. Both DI_{rms} and DI_{var} are measured within all damage cases. The result shows corresponding increment under l_c, as shown in **Figure 3(c)**.

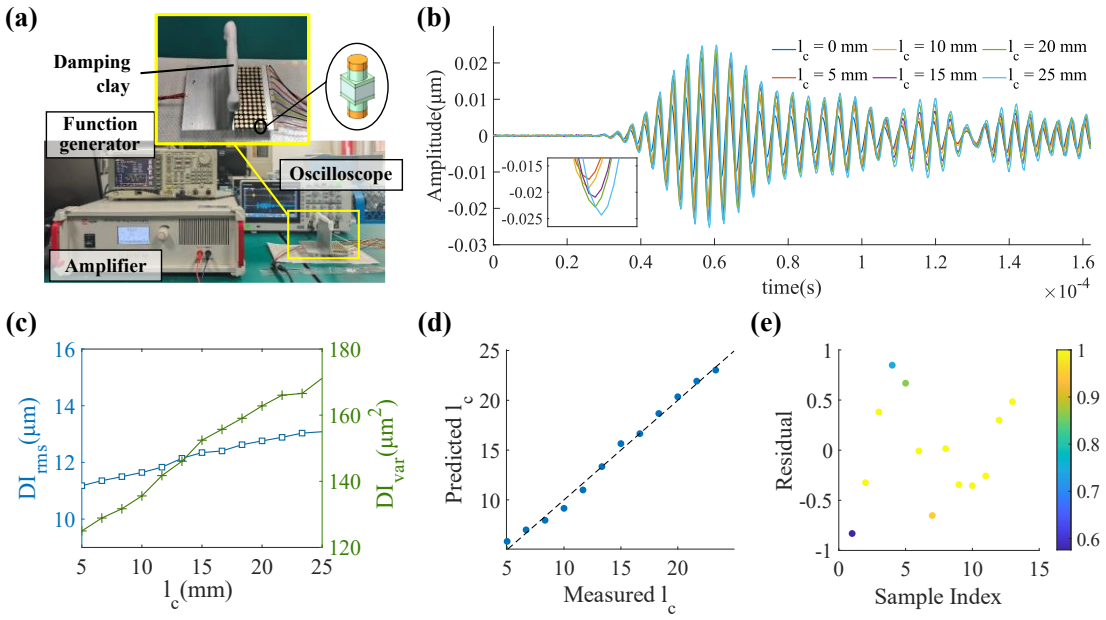

Figure 3 Experimental setting and result, including (a) testbench layout, (b) signals captured under different l_c, (c) DI_{rms} and DI_{var} values under different l_c, (d) regression effect of response model by $\widehat{l_c}$ vs l_c and (e) weight and residual value of all samples.

B. Baseline Discontinuity Size Quantification

To quantify the discontinuity length, a regression model with the damage index as model independent variables is proposed. Previous study [9] shows that multifeatured quantification facilitates the evaluation accuracy. A response surface model incorporating the DI_{rms}, DI_{var} and the interaction between the two is established as

$$l_c = a_0 + a_1 DI_{\text{rms}} + a_2 DI_{\text{var}} + a_3 DI_{\text{rms}} \cdot DI_{\text{var}} \tag{9}$$

It should be noted that the damage sensitive features $\mathbf{D} = [DI_{\text{rms}}, DI_{\text{var}}]$ have specific physical meaning, and the baseline model obtained using experimental data reflects a phenomenal interaction of Lamb wave with discontinuity from an experiment point of view. In this condition, uncertainty is introduced by the nondeterministic framework, causing abnormal data points. As a result, the model of

Huber Regression (HR) estimator is used to identify parameter statistically [10]. The Huber loss is defined such that the penalty impact is weakened when the residual is larger than the threshold,

$$L_\delta(r) = \begin{cases} \frac{1}{2}r^2 & if\ |r| \le \delta \\ \delta\left(|r| - \frac{1}{2}\delta\right) & if\ |r| > \delta \end{cases} \tag{10}$$

in which, r is the calculated loss, δ is the preset threshold. The threshold is set by z-score criteria as $\delta = z\sigma + \mu$. In this research, z is set as 1.5 and μ, σ is the mean value and variance of every loss. The optimization target is defined as

$$\boldsymbol{\alpha} = \min_{\boldsymbol{\alpha}} \sum_{i=1}^{n} L_\delta(r)\left(l_{c,i} - \mathbf{D}_i^T\boldsymbol{\alpha}\right) + \lambda\|\boldsymbol{\alpha}\|_2^2 \tag{11}$$

in which, $\boldsymbol{\alpha} = [a_0,\ a_1,\ a_2,\ a_3]$ is the parametric array; $\mathbf{D} = [DI_{\text{rms}},\ DI_{\text{var}}]$ is the training input. Iteratively Reweighted Least Squares (IRLS) method [11] is introduced to solve **Equation 11**.

The regression effect of response model and the sample weights are presented in **Figure 3(d) and 3(e).** A deterministic baseline model can be expressed using the mean vector of $\boldsymbol{\alpha}$ as

$$l_c = 47.45 - 5.06DI_{\text{rms}} - 0.66DI_{\text{var}} + 0.07DI_{\text{rms}} \cdot DI_{\text{var}} \tag{9}$$

The Huber estimator demonstrates strong extensibility when applied to fitting real-world phenomena, especially if future cases are measured and added into the model.

CONCLUSION

This study proposes a novel SHM framework using ultrasonic guided wave mode discrimination combined with acoustic metamaterials for integrity monitoring of right-angle structures. Key findings include the observation that S0 to A0 mode transitions at geometric discontinuities significantly affect defect detection sensitivity. Introducing a metasurface with a specifically designed bandgap effectively filtered out dominant A0 mode energy, amplifying defect-sensitive S0 mode signals. Finite element simulations confirmed a substantial stress reduction of at least five orders of magnitude for the A0 mode within its bandgap (244 kHz), enhancing defect detection capabilities. Experimental validation on a T-shaped aluminum structure demonstrated clear amplitude increases correlated with defect length increments (5–25 mm), with root mean square and variance-based damage indices providing precise quantitative defect evaluation. The Huber regression model further enhanced reliability, accurately correlating measured signals with discontinuity lengths, demonstrating strong practical applicability and extensibility for future structural integrity monitoring applications.

REFERENCES

[1] A. Sofi, J. Jane Regita, B. Rane, and H. H. Lau, 'Structural health monitoring using wireless smart sensor network – An overview', *Mechanical Systems and Signal Processing*, vol. 163, p. 108113, Jan. 2022, doi: 10.1016/j.ymssp.2021.108113.

[2] Z. Su, L. Ye, and Y. Lu, 'Guided Lamb waves for identification of damage in composite structures: A review', *Journal of Sound and Vibration*, vol. 295, no. 3–5, pp. 753–780, Aug. 2006, doi: 10.1016/j.jsv.2006.01.020.

[3] Younho Cho, 'Estimation of ultrasonic guided wave mode conversion in a plate with thickness variation', *IEEE Trans. Ultrason., Ferroelect., Freq. Contr.*, vol. 47, no. 3, pp. 591–603, May 2000, doi: 10.1109/58.842046.

[4] V. Serey, N. Quaegebeur, P. Micheau, P. Masson, M. Castaings, and M. Renier, 'Selective generation of ultrasonic guided waves in a bi-dimensional waveguide', *Structural Health Monitoring*, vol. 18, no. 4, pp. 1324–1336, Jul. 2019, doi: 10.1177/1475921718808220.

[5] Z. Liu, S. Shan, and L. Cheng, 'Meta-structure enhanced second harmonic S0 waves for material microstructural changes monitoring', *Ultrasonics*, vol. 139, p. 107295, Apr. 2024, doi: 10.1016/j.ultras.2024.107295.

[6] D. Du, J. Hua, C. Cui, and J. Lin, 'Energy focusing of broadband Lamb wave by designing excitation waveforms and elastic metamaterials', *Ultrasonics*, vol. 139, p. 107294, Apr. 2024, doi: 10.1016/j.ultras.2024.107294.

[7] Y. Tian, H. Fu, and Y. Shen, 'An elastic meta-enhancer for improved damage detection via nonlinear ultrasonic feature amplification', *Mechanical Systems and Signal Processing*, vol. 231, p. 112685, May 2025, doi: 10.1016/j.ymssp.2025.112685.

[8] Y. Tian and Y. Shen, 'Selective guided wave mode transmission enabled by elastic metamaterials', *Journal of Sound and Vibration*, vol. 485, p. 115566, Oct. 2020, doi: 10.1016/j.jsv.2020.115566.

[9] W. Liu, Z. Tang, F. Lv, and X. Chen, 'Multi-feature integration and machine learning for guided wave structural health monitoring: Application to switch rail foot', *Structural Health Monitoring*, vol. 20, no. 4, pp. 2013–2034, Jul. 2021, doi: 10.1177/1475921721989577.

[10] K. M. Tan, Q. Sun, and D. Witten, 'Sparse Reduced Rank Huber Regression in High Dimensions', *Journal of the American Statistical Association*, vol. 118, no. 544, pp. 2383–2393, Oct. 2023, doi: 10.1080/01621459.2022.2050243.

[11] P. Zhang, B. Liu, and J. Pan, 'Iteratively Reweighted Least Squares Method for Estimating Polyserial and Polychoric Correlation Coefficients', *Journal of Computational and Graphical Statistics*, vol. 33, no. 1, pp. 316–328, Jan. 2024, doi: 10.1080/10618600.2023.2257251.